







ORIGINAL RESEARCH

Magnetic Resonance Imaging-Derived Microvascular Perfusion Modeling to Assess Peripheral Artery Disease

Olga A. Gimnich, PhD; Tatiana Belousova, MD; Christina M. Short, MBA; Addison A. Taylor , MD, PhD; Vijay Nambi , MD, PhD; Joel D. Morrisett, PhD; Christie M. Ballantyne , MD; Jean Bismuth , MD; Dipan J. Shah , MD; Gerd Brunner , MS, PhD

BACKGROUND: Computational fluid dynamics has shown good agreement with contrast-enhanced magnetic resonance imaging measurements in cardiovascular disease applications. We have developed a biomechanical model of microvascular perfusion using contrast-enhanced magnetic resonance imaging signal intensities derived from skeletal calf muscles to study peripheral artery disease (PAD).

METHODS AND RESULTS: The computational microvascular model was used to study skeletal calf muscle perfusion in 56 individuals (36 patients with PAD, 20 matched controls). The recruited participants underwent contrast-enhanced magnetic resonance imaging and ankle-brachial index testing at rest and after 6-minute treadmill walking. We have determined associations of microvascular model parameters including the transfer rate constant, a measure of vascular leakiness; the interstitial permeability to fluid flow which reflects the permeability of the microvasculature; porosity, a measure of the fraction of the extracellular space; the outflow filtration coefficient; and the microvascular pressure with known markers of patients with PAD. Transfer rate constant, interstitial permeability to fluid flow, and microvascular pressure were higher, whereas porosity and outflow filtration coefficient were lower in patients with PAD than those in matched controls (all P values ≤ 0.014). In pooled analyses of all participants, the model parameters (transfer rate constant, interstitial permeability to fluid flow, porosity, outflow filtration coefficient, microvascular pressure) were significantly associated with the resting and exercise ankle-brachial indexes, claudication onset time, and peak walking time (all P values ≤ 0.013). Among patients with PAD, interstitial permeability to fluid flow, and microvascular pressure were higher, while porosity and outflow filtration coefficient were lower in treadmill noncompleters compared with treadmill completers (all P values ≤ 0.001).

CONCLUSIONS: Computational microvascular model parameters differed significantly between patients with PAD and matched controls. Thus, computational microvascular modeling could be of interest in studying lower extremity ischemia.

Key Words: computational microvascular model ■ magnetic resonance imaging ■ microvascular perfusion ■ peripheral artery disease

Peripheral artery disease (PAD) is a vascular disease accompanied by atherosclerotic lesions and is associated with an increased risk of cardiovascular events and mortality.^{1,2} PAD is characterized by impaired muscle function, and diabetes is common in individuals with lower extremity ischemia.^{3,4} Improving microvascular perfusion of the leg muscles and

alleviating intermittent claudication remain a challenge in patients with PAD, as present surgical and therapeutic treatments are not successful in relieving symptoms in all patients with lower extremity ischemia.^{5–8} A previous report¹ showed that contrast-enhanced magnetic resonance imaging (CE-MRI) permits studying microvascular muscle perfusion in patients with PAD and

Correspondence to: Gerd Brunner, MS, PhD, Penn State Heart and Vascular Institute 500 University Dr H047, Hershey, PA 17033. Email: gbrunner@pennstatehealth.psu.edu

Supplemental Material is available at <https://www.ahajournals.org/doi/suppl/10.1161/JAHA.122.027649>

For Sources of Funding and Disclosures, see page 10.

© 2023 The Authors. Published on behalf of the American Heart Association, Inc., by Wiley. This is an open access article under the terms of the [Creative Commons Attribution-NonCommercial-NoDerivs](#) License, which permits use and distribution in any medium, provided the original work is properly cited, the use is non-commercial and no modifications or adaptations are made.

JAHA is available at: www.ahajournals.org/journal/jaha

CLINICAL PERSPECTIVE

What Is New?

- Computational microvascular model parameters differed significantly between patients with peripheral artery disease and matched controls.
- Computational microvascular modeling could be of interest in studying lower extremity ischemia.

What Are the Clinical Implications?

- This work adds to the growing body of evidence on the importance of the microcirculation in peripheral artery disease, and the presented computational microvascular model provides a potential tool to elucidate associations between the microcirculation and peripheral artery disease symptoms.

Nonstandard Abbreviations and Acronyms

P_v	microvascular pressure
AM	anterior muscle group
DM	deep posterior muscle group
GBCA	gadolinium-based contrast agent
GM	gastrocnemius muscle
k^t	transfer rate constant
K_{tissue}	interstitial permeability to fluid flow
LM	lateral muscle group
OFC	outflow filtration coefficient
SM	soleus muscle
φ	porosity

could be of clinical interest in assessing PAD severity. Computational fluid dynamics has shown good agreement with CE-MRI measurements in cardiovascular disease applications^{9–11} and could be an important tool for studying tissue perfusion.^{12–14} A biomechanical model of microvascular perfusion in patients with PAD¹⁵ was developed using CE-MRI signal intensities derived from 5 distinct calf muscle regions, including the anterior muscle group (AM), lateral muscle group (LM), deep posterior muscle group (DM), soleus muscle (SM), and gastrocnemius muscle (GM). The model was robust and can be used to estimate microvascular transport properties in the calf muscles. The present study aimed to determine tissue perfusion parameters and compare tissue transport properties between patients with PAD and matched controls, along with estimates of changes in tissue transport properties depending on disease severity or concomitant diabetes. The primary purpose of this study was to investigate

whether parameters from a biomechanical model of microvascular perfusion based on CE-MRI are associated with known markers of PAD and can be used to differentiate between patients with PAD and matched controls. In addition, we sought to determine whether the parameters from the biomechanical model of microvascular perfusion can differentiate between PAD treadmill-completers and noncompleters.

METHODS

In accordance with the American Heart Association journals' implementation of the Transparency and Openness Promotion Guidelines, the data supporting the findings of this study are available from the corresponding author upon reasonable request. Study participants provided informed consent, and the study obtained approval from the local institutional review board. Patients with PAD and controls were recruited from the Houston Methodist Hospital and the Michael E. DeBakey Veterans Affairs Medical Center, Houston, TX, as described previously.^{1,16} The study details and baseline characteristics of the same participants have been reported previously.¹⁶ Briefly, adults with a resting ankle-brachial index (ABI) <0.9, a lifestyle-limiting intermittent claudication, and an estimated glomerular filtration rate >40 mL/min per 1.73 m² but without contraindications to magnetic resonance imaging (MRI) were included in this study. Controls without PAD were matched for age, sex, and body mass index. To achieve balanced enrollment, we periodically performed statistical testing of the matching variables (age, sex, body mass index) between the patients with PAD and controls using an independent sample Student *t*-test or a Chi-square test. Study participants underwent ABI measurements at rest and after a 6-minute graded treadmill walking test, as reported previously.¹⁶

Magnetic Resonance Imaging

A 3.0-T system (Siemens Magnetom Trio, or Verio, Erlangen, Germany) with a 36-element bilateral lower extremity coil was used for CE-MRI with a gadolinium-based contrast agent (GBCA). After initial localizers, muscle perfusion imaging was performed at the mid-calf level, as described previously.¹ Briefly, a reactive hyperemia protocol was implemented by using MRI compatible bilateral blood-pressure cuffs that were placed above the knee and inflated to supra-systolic pressure levels (170 mmHg) for 3.5 minutes. Following rapid cuff deflation and the GBCA administration, perfusion imaging was performed immediately using a high-resolution saturation recovery gradient echo pulse sequence (repetition time/echo time=2.7/1.23 ms; field of view=17.5×35.0 cm; slice thickness=10 mm, temporal resolution (perfusion imaging frame rate)=409 ms).

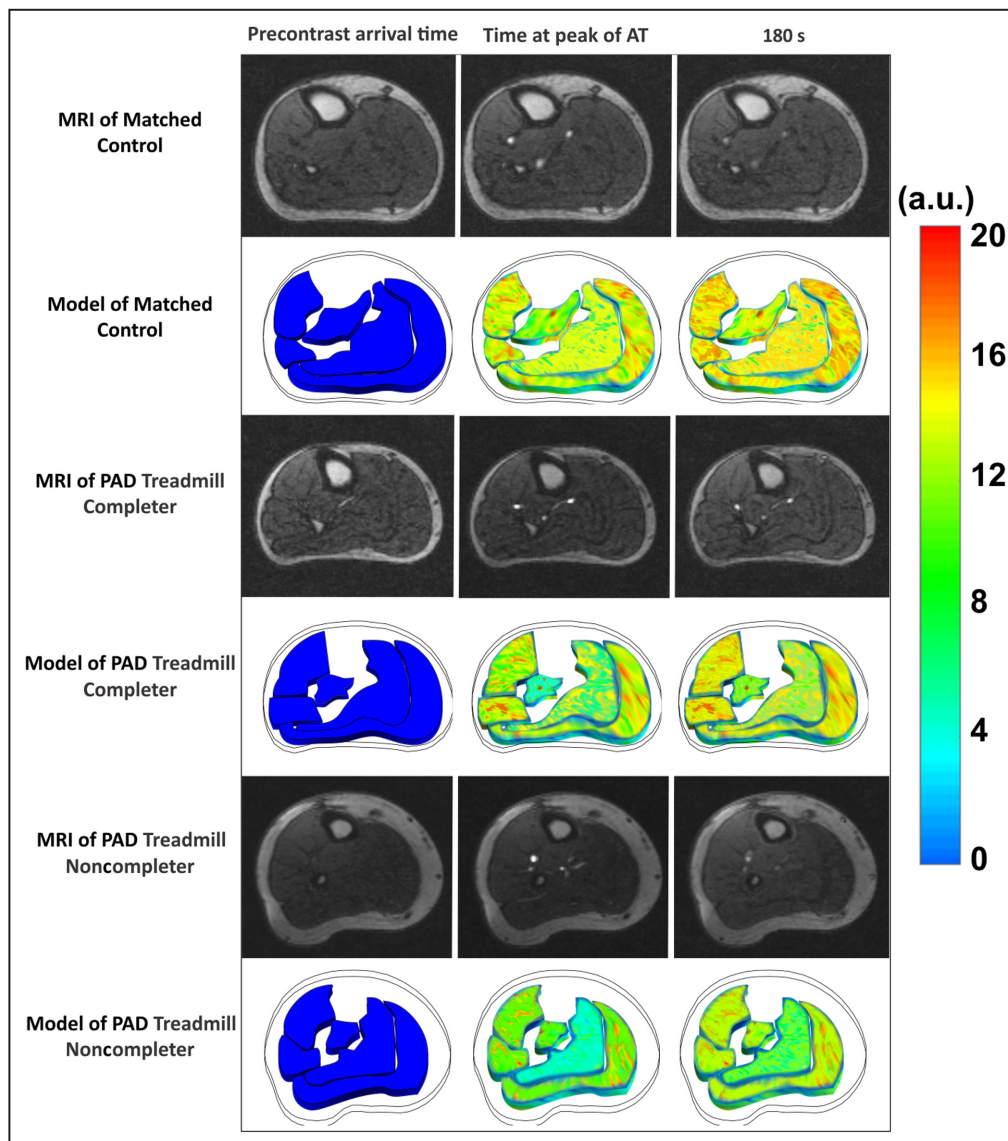


Figure. Contrast-enhanced magnetic resonance imaging and corresponding simulated signal intensities from the computational microvascular model for a matched-control, a treadmill completer with peripheral artery disease, and a treadmill noncompleter with peripheral artery disease.

Specific time points are shown including before contrast arrival, peak arterial enhancement of the anterior tibial artery, and after 180 seconds. The panels of the computational microvascular model include 5 distinct skeletal calf muscle compartments (anterior muscle, lateral muscle, deep posterior muscle, soleus muscle, and the gastrocnemius muscle). A.U. indicates arbitrary units; AT, anterior tibial artery; MRI, magnetic resonance imaging; and PAD, peripheral artery disease.

Image Analysis

The acquired CE-MRI data sets saved in DICOM format had a slice thickness of 10 mm and a temporal resolution of 409 ms. The MRI scans were anonymized before analysis. Calf muscle domains, including AM, LM, DM, SM, and GM were semi-automatically segmented using an in-house graphical user interface developed in MATLAB (MathWorks Natick, MA). The arterial lumen of the posterior tibialis, anterior tibialis and

peroneal arteries were segmented with Sante DICOM Editor Version 3.0 (Santesoft LTD, Greece). Additional details about the segmentation algorithm were previously described.^{1,16} The peak arterial signal, the minimum post-peak enhancement, and the level of arterial signal enhancement were extracted for each of the 3 main arteries (posterior tibialis, anterior tibialis, and peroneal arteries), and the cross-sectional leg muscle area was measured, as described previously.¹

Table 1. Baseline Patient Characteristics

Variable	Patients with PAD (n=36)	Controls (n=20)	P value
Age, y	69±9.0	65±6.7	0.10
Men, %	27 (75%)	12 (60%)	0.36
Race, % Black	12 (33%)	4 (20%)	0.36
Body mass index, kg/m ²	27±4.9	29±5.3	0.19
Resting ABI, A.U.	0.75±0.2	1.17±0.1	<0.001
Post-treadmill ABI, A.U.	0.60 (0.5–0.7)	1.19 (1.1–1.2)	<0.001
Smoker, %	32 (89%)	8 (40%)	<0.001
Diabetes, %	17 (47%)	3 (15%)	0.021
Hypertension, %	33 (92%)	12 (60%)	0.011
Hyperlipidemia, %	34 (94%)	12 (60%)	0.002
Heart rate, bpm	78±19	71±10	0.13
Hematocrit, %	41 (39–42)	41 (40–44)	0.46
eGFR, ml/min per 1.73m ²	78±22	78±18	0.95
ACE inhibitor, %	17 (47%)	5 (25%)	0.15
Beta-blocker, %	18 (50%)	7 (35%)	0.40
Claudication onset time, s	222 (180–264)	353 (346–360)	<0.001
Peak walking time, s	282 (248–317)	353 (346–360)	0.002
Complete 6-min treadmill, %	19 (53%)	19 (95%)	0.002
Cholesterol-lowering drug use, %	32 (89%)	9 (45%)	0.001
Coronary artery disease, %	15 (42%)	5 (25%)	0.26
Lower extremity revascularization history, %	22 (61%)	0 (0%)	0.001
Family history of coronary heart disease, %	14 (39%)	8 (40%)	0.07

Values are reported as mean±SD, median (interquartile range), and number (percentage). Hematocrit controls: n=15; post-treadmill ankle-brachial index patients with peripheral artery disease: n=35; claudication onset time patients with peripheral artery disease: n=35; peak walking time patients with peripheral artery disease: n=35. The baseline characteristics of the same participants have been reported previously.¹⁶ ABI indicates ankle-brachial index; A.U., arbitrary units; eGFR, estimated glomerular filtration rate; and PAD, peripheral artery disease.

Biomechanical Modeling: Computational Microvascular Model

The validated biomechanical model for calf muscle microvascular perfusion was reported previously.¹⁵ Briefly, the ANSYS SpaceClaim application within the ANSYS Workbench (Ansys, Inc, v. 18.2) was used for creating 3-dimensional volumes of leg segments with a thickness of 10mm to maintain continuity and clinical relevance (same thickness as CE-MRI scans). The 2-compartment Tofts-Kermode model¹⁷ of plasma and tissue was taken as the basis of our computational microvascular model, which was used to describe the CE-MR signal enhancement by GBCA as a reaction term in the tissue regions. The convection-diffusion and reaction models were adopted to simulate 3-dimensional convection-enhanced delivery in the tissue regions.¹⁸ The skeletal muscle tissue was modeled as a porous media using the user-defined model of elastic solid tissue with a porosity of 20% to 80% (Figure).

The primary microvascular model parameters include the transfer rate constant (k^t),^{15,19,20} a measure of vascular leakiness; the interstitial permeability to fluid flow (K_{tissue})^{15,19,20} which reflects the permeability of the microvasculature that is modeled as a porous

medium²⁰; porosity (ϕ),^{15,20,21} a measure of the fraction of the extracellular space or tissue porosity; the out-flow filtration coefficient (OFC)^{15,20}; and the microvascular pressure (p_v).^{15,20,22} The OFC is the product of the vessel permeability and the microvascular surface area per unit volume.^{15,20} Further details of the computational microvascular model were reported previously.¹⁵

Parameters of the finite element model were calculated using the programming method implemented in the ANSYS software (v. 18.2). The developed full porous model is a generalization of the Navier–Stokes equations and Darcy law commonly used for flows in porous regions. Blood perfusion velocity and pressure were determined and described for each muscle domain. Blood perfusion was assumed to be transient, incompressible flow. On the boundaries, mass sources were applied to introduce additional fluid into the simulation. The arterial input function corresponding to the signal intensity of the contrast agent in the blood plasma was obtained from CE-MRI scans¹ and applied as a boundary condition for the suggested biomechanical model. Furthermore, a relative static pressure of zero was specified over the outlet boundary, and the flow velocity at the wall boundary was also

Table 2. Computational Microvascular Model Parameters for Matched Controls and Patients With PAD

Variable	Control	PAD	Pooled	P value
k^t , 1/s	2.45 (2.28–2.62)	7.09 (5.86–8.31)	5.43 (4.45–6.41)	<0.001
K_{tissue} , m^2	1.81 (1.81–1.81)	4.31 (4.03–4.60)	3.42 (3.05–3.79)	<0.001
φ	0.67 (0.65–0.69)	0.47 (0.44–0.49)	0.54 (0.51–0.57)	<0.001
OFC, 1/Pa s	13.37 (12.16–14.58)	11.10 (9.92–12.28)	11.91 (11.01–12.81)	0.014
p_v , mmHg	49.21 (48.74–49.67)	52.53 (51.65–53.41)	51.34 (50.64–52.06)	<0.001

All values are expressed as median (interquartile range). *P* values were calculated with the Kruskal–Wallis rank test. Control group: *n*=20; peripheral artery disease group: *n*=36. Pooled: includes both patients with PAD and controls. k^t indicates transfer rate constant; K_{tissue} , interstitial permeability; OFC, outflow filtration coefficient; PAD, peripheral artery disease; p_v , microvascular pressure; and φ , porosity (values in the range from 0 to 1).

set to zero. Full information about model parameters is available in our previous publication.¹⁵ The grid test and transient time step sensitivity tests were performed to check the quality of the model and for solution convergence. Mean square and mean absolute percentage errors were calculated to estimate the best agreement between simulated and CE-MRI signal intensities. Intrarater and interrater (for 3 patients with PAD and 5 controls) reproducibility for simulated mean signal intensity over all time steps was excellent for all muscle groups, as reported previously.¹⁵

Statistical Analysis

Statistical analyses were performed with Stata IC 13.1 (College Station, Texas, StataCorp LP). All variables were expressed as means, or medians along with a measure of variability (SD, interquartile range,

frequencies, or percentages). The Shapiro–Wilk test was used to check for variable normality. An independent sample Student *t* test was used for continuous variables, and the Mann–Whitney–Wilcoxon test was used for non-normal variables. Pearson correlation analyses were performed, and the strength of the correlation was described as weak ($r<0.3$), medium ($0.3\leq r<0.5$), or strong ($r\geq 0.5$). Associations between computational microvascular model parameters and markers of PAD were determined using linear regression analysis. The chi-square or Fisher exact test was used to analyze group differences in categorical variables. Variables were compared between patients with PAD and matched controls, PAD treadmill completers and PAD noncompleters, and diabetic and nondiabetic study participants. All tests were 2-sided, and a *P* value <0.05 was considered statistically significant.

Table 3. Correlation Analyses of Markers of PAD With Computational Microvascular Modeling Parameters

Variable	Group	Obs	k^t	K_{tissue}	φ	OFC	p_v	
Age	Control	<i>r</i>	20	0.32	0.19	0.10	–0.22	0.10
		<i>P</i> value		0.17	0.42	0.68	0.35	0.67
	PAD	<i>r</i>	36	–0.05	0.14	–0.13	–0.03	0.01
		<i>P</i> value		0.77	0.43	0.46	0.86	0.95
	Pooled	<i>r</i>	56	0.11	0.25	–0.23	0.14	0.15
		<i>P</i> value		0.42	0.06	0.08	0.30	0.27
Body mass index	Control	<i>r</i>	20	–0.10	0.01	0.10	0.24	–0.20
		<i>P</i> value		0.67	0.95	0.67	0.32	0.39
	PAD	<i>r</i>	36	–0.13	0.02	0.03	–0.01	0.11
		<i>P</i> value		0.47	0.90	0.88	0.96	0.52
	Pooled	<i>r</i>	56	–0.19	–0.15	0.17	0.12	–0.07
		<i>P</i> value		0.16	0.28	0.21	0.39	0.62
eGFR	Control	<i>r</i>	20	0.24	–0.09	–0.03	–0.09	0.02
		<i>P</i> value		0.30	0.70	0.91	0.71	0.94
	PAD	<i>r</i>	36	–0.02	0.24	0.02	–0.08	0.16
		<i>P</i> value		0.92	0.17	0.93	0.66	0.36
	Pooled	<i>r</i>	56	<0.01	0.11	<0.01	–0.08	0.11
		<i>P</i> value		1.00	0.43	0.99	0.58	0.41

Pooled, includes both patients with peripheral artery disease and controls. eGFR indicates estimated glomerular filtration rate; k^t , transfer rate constant; K_{tissue} , interstitial permeability; Obs, number of observations; OFC, outflow filtration coefficient; PAD, peripheral artery disease; p_v , microvascular pressure; and φ , porosity.

RESULTS

Baseline Characteristics

A total of 66 participants were enrolled, and 61 patients completed the baseline MRI visit. Five patients were excluded because of incomplete MRI due to poor image quality ($n=4$), or incomplete ABI data ($n=1$). In the final analysis, 56 participants were included (36 PAD, 20 controls). The baseline characteristics of the same participants have been reported previously and are summarized here next.¹⁶ There were no differences in age, sex, race, or body mass index between patients with PAD and matched controls (Table 1). Compared with controls, patients with PAD were more likely to be diabetic (47% versus 15%, $P=0.021$), hypertensive (92% versus 60%, $P=0.011$), hyperlipidemic (94% versus 60%, $P=0.002$), and on lipid-lowering therapy (89% versus 45%, $P=0.001$). Furthermore, more patients with PAD had a history of lower extremity revascularization (61% versus 0%, $P=0.001$) and were smokers (89% versus 40%, $P<0.001$) than controls.

Please note that the same findings about the ABIs and the treadmill walking parameters have been reported before and are summarized below.¹⁶ Resting ABIs were significantly lower (0.75 ± 0.2 versus 1.17 ± 0.1 , $P<0.001$), whereas the peak walking time (PWT) was shorter (282 [248–317] seconds versus 353 [346–360] seconds, $P=0.002$) for patients with PAD than those for matched controls (Table 1). The ABIs decreased significantly post-treadmill walking in patients with PAD but not in controls, as expected ($P<0.001$ versus $P=0.50$, Table 1).

In a subgroup analysis, patients with PAD were divided into 2 groups: (1) those who completed the 6-minute treadmill walking test, and (2) those who did not, as reported previously (treadmill completers, $n=19$; treadmill noncompleters, $n=17$).¹⁶ Treadmill completers had lower resting ABIs (0.65 ± 0.2 versus 0.84 ± 0.2 , $P=0.011$), a shorter PWT (190 [148–232] seconds versus 360 [360–360] seconds, $P<0.001$), and a shorter claudication onset time (122 [80–164] seconds versus 232 [163–301] seconds, $P=0.005$), when compared with noncompleters, as reported before.¹⁶

Computational Microvascular Model Parameters

Averaged over all muscle groups, k^t , K_{tissue} , and p_v were higher in patients with PAD than in controls (all P values <0.001 , Table 2). Porosity and the OFC averaged over all muscle groups were lower in patients with PAD than in controls (all P values <0.015 , Table 2).

Modeling parameters were heterogeneous across individual calf muscle groups. Compared with controls, patients with PAD had significantly higher k^t and K_{tissue} values in all 5 muscle groups (Table S1 through

S3). Similarly, p_v was significantly higher in the LM ($P=0.006$), DM ($P<0.001$), and GM ($P=0.005$) of patients with PAD than that in the corresponding muscle groups of the controls but was similar in the AM and SM. Furthermore, φ was significantly lower in patients with PAD than in controls in all 5 muscle groups ($P<0.001$). The OFC was significantly lower in the AM of patients with PAD than in the AM of controls ($P=0.001$) but not in other muscle groups.

Correlation of Patient Characteristics With Computational Microvascular Model Parameters

There were no significant correlations between age, BMI, and the eGFR with the computational microvascular model parameters (Table 3).

Associations of Computational Microvascular Model Parameters With Markers of PAD

The parameters k^t , K_{tissue} , φ , OFC, and p_v were significantly associated with the resting ABI, post-treadmill ABI, claudication onset time, and PWT in the pooled analysis comprising all study participants (all P values ≤ 0.013 , Table 4). K_{tissue} and φ were significantly associated with the difference in the ABI ($P=0.006$; $P=0.010$) of the pooled analysis. In separate analyses, only among patients with PAD, but not among controls, K_{tissue} , φ , OFC, and p_v were significantly associated with claudication onset time and PWT (Table 5). Conversely, k^t was associated with the post-treadmill ABI, and the OFC was associated with the resting ABI in controls but not in patients with PAD (Table 6).

Computational Microvascular Model Parameters in Subgroup Analysis

Averaged over all muscle groups, K_{tissue} and p_v were higher in patients with diabetes and PAD than in patients with PAD without diabetes (Table 7). k_{tissue} was significantly higher in the AM ($P=0.005$), LM ($P=0.009$), DM ($P=0.009$), and SM ($P=0.023$) of patients with diabetes and PAD compared with the corresponding muscles of those without diabetes. p_v was significantly higher in patients with PAD and diabetes than in patients without diabetes for the DM ($P=0.005$) but not for the other muscle groups. Parameter φ was significantly lower in the GM of patients with diabetes and PAD than in patients with PAD without diabetes ($P=0.026$) but not in other muscle groups (Table S2).

K_{tissue} and p_v were significantly higher in treadmill noncompleters than in treadmill completers when averaged over all muscle groups (both P values <0.001 ,

Table 4. Associations of Computational Microvascular Modeling Parameters With Markers of PAD

Variable	Independent variable	Obs	β	SE	R^2	Adjusted r^2	P value
k^t	Resting ABI	56	-0.032	0.0093	0.18	0.16	0.001
	Post-treadmill ABI	55	-0.043	0.0120	0.20	0.18	0.001
	Δ of ABI	55	-0.012	0.0069	0.05	0.03	0.10
	Claudication onset time, s	55	-16.67	3.7337	0.27	0.26	<0.001
	Peak walking time, s	55	-8.258	3.0860	0.12	0.10	0.010
K_{tissue}	Resting ABI	56	-0.129	0.0205	0.42	0.41	<0.001
	Post-treadmill ABI	55	-0.178	0.0259	0.47	0.46	<0.001
	Δ of ABI	55	-0.050	0.0177	0.13	0.12	0.006
	Claudication onset time, s	55	-54.93	8.8906	0.42	0.41	<0.001
	Peak walking time, s	55	-43.75	6.3649	0.47	0.46	<0.001
φ	Resting ABI	56	1.634	0.2235	0.50	0.49	<0.001
	Post-treadmill ABI	55	2.185	0.2918	0.51	0.50	<0.001
	Δ of ABI	55	0.560	0.2097	0.12	0.10	0.010
	Claudication onset time, s	55	776.8	86.325	0.60	0.60	<0.001
	Peak walking time, s	55	542.6	71.138	0.52	0.51	<0.001
OFC	Resting ABI	56	0.027	0.0105	0.11	0.09	0.013
	Post-treadmill ABI	55	0.037	0.0137	0.12	0.10	0.009
	Δ of ABI	55	0.011	0.0077	0.04	0.02	0.15
	Claudication onset time, s	55	18.33	4.0849	0.28	0.26	<0.001
	Peak walking time, s	55	16.64	2.7839	0.40	0.39	<0.001
p_v	Resting ABI	56	-0.049	0.0122	0.23	0.22	<0.001
	Post-treadmill ABI	55	-0.056	0.0164	0.18	0.17	0.001
	Δ of ABI	55	-0.008	0.0096	0.01	-0.01	0.43
	Claudication onset time, s	55	-28.65	4.4608	0.44	0.43	<0.001
	Peak walking time, s	55	-18.72	3.6501	0.33	0.32	<0.001

Linear regression analyses were performed for all included individuals (pooled). ABI indicates ankle-brachial index; k^t , transfer rate constant; K_{tissue} , interstitial permeability; Obs, number of observations; OFC, outflow filtration coefficient; PAD, peripheral artery disease; p_v , microvascular pressure; Δ of ABI, difference between resting ankle-brachial index and post-treadmill ankle-brachial index; and φ , porosity.

Table 8). Averaged over all muscle groups, φ and the OFC were significantly lower in treadmill noncompleters versus treadmill completers (both P values <0.001, Table 8). Compared with treadmill completers, treadmill noncompleters had significantly higher k^t values in the DM (P <0.001) and SM (P <0.001); however, no differences in k^t were found for the AM, LM, and GM (Table S3). K_{tissue} was significantly higher in the AM (P =0.005), LM (P =0.004), SM (P =0.009), and GM (P <0.001) of treadmill noncompleters compared with the corresponding values of treadmill completers but was not different for the DM. Similarly, treadmill noncompleters had a significantly higher p_v in the DM (P =0.007) and GM (P =0.002) than treadmill completers but not in the AM, LM, and SM. Furthermore, φ was significantly lower in all 5 muscle groups in treadmill noncompleters compared with treadmill completers. The OFC was significantly lower in the LM (P =0.008),

DM (P =0.033), SM (P <0.001), and GM (P <0.001) of treadmill noncompleters compared with that of treadmill completers but did not differ in the AM for both groups.

DISCUSSION

Using numerical modeling based on CE-MRI signal intensities, we determined muscle perfusion properties depending on PAD severity and concomitant diabetes. There were 5 main findings in this study. First, averaged over all muscle groups, k^t , K_{tissue} , and p_v were significantly higher while φ and the OFC were significantly lower in patients with PAD compared with the corresponding parameters in matched controls. Second, tissue permeability was significantly higher across distinct muscle regions in patients with PAD than in controls, and φ was heterogeneous across

Table 5. Associations of Computational Microvascular Modeling Parameters From Patients With PAD With Markers of PAD

Variables	Independent variable	Obs	<i>B</i>	SE	<i>R</i> ²	Adjusted <i>r</i> ²	<i>P</i> value
<i>k</i> ^t	Resting ABI	36	0.002	0.0107	0.00	−0.03	0.82
	Post-treadmill ABI	35	0.006	0.0124	0.01	−0.02	0.64
	Δ of ABI	35	0.004	0.0091	0.00	−0.03	0.70
	Claudication onset time, s	35	−9.431	5.5899	0.08	0.05	0.10
	Peak walking time, s	35	−3.712	4.7367	0.02	−0.01	0.44
<i>K</i> _{tissue}	Resting ABI	36	−0.012	0.0459	0.00	−0.03	0.79
	Post-treadmill ABI	35	0.010	0.0537	0.00	−0.03	0.86
	Δ of ABI	35	0.018	0.0393	0.01	−0.02	0.65
	Claudication onset time, s	35	−59.01	22.883	0.17	0.14	0.015
	Peak walking time, s	35	−89.50	13.448	0.57	0.56	<0.001
φ	Resting ABI	36	0.940	0.4563	0.11	0.08	0.047
	Post-treadmill ABI	35	0.761	0.5579	0.05	0.02	0.18
	Δ of ABI	35	−0.145	0.4199	0.00	−0.03	0.73
	Claudication onset time, s	35	1116.3	184.08	0.53	0.51	<0.001
	Peak walking time, s	35	1014.7	130.53	0.65	0.64	<0.001
OFC	Resting ABI	36	0.004	0.0111	0.00	−0.02	0.70
	Post-treadmill ABI	35	0.009	0.0129	0.01	−0.02	0.49
	Δ of ABI	35	0.006	0.0095	0.01	−0.02	0.57
	Claudication onset time, s	35	17.40	5.2504	0.25	0.23	0.002
	Peak walking time, s	35	18.98	3.7169	0.44	0.42	<0.001
<i>p</i> _v	Resting ABI	36	−0.007	0.0148	0.01	−0.02	0.66
	Post-treadmill ABI	35	0.013	0.0172	0.02	−0.01	0.47
	Δ of ABI	35	0.019	0.0122	0.07	0.04	0.12
	Claudication onset time, s	35	−24.09	6.9062	0.27	0.25	0.001
	Peak walking time, s	35	−18.23	5.8204	0.23	0.21	0.004

Linear regression analyses were performed for patients with PAD. ABI indicates ankle-brachial index; *k*^t, transfer rate constant; *K*_{tissue}, interstitial permeability; Obs, number of observations; OFC, outflow filtration coefficient; PAD, peripheral artery disease; *p*_v, microvascular pressure; Δ of ABI, difference between resting ankle-brachial index and post-treadmill ankle-brachial index; and φ, porosity.

muscle groups. Third, *K*_{tissue} and *p*_v were significantly higher in patients with diabetes and PAD than in patients with PAD without diabetes. Fourth, *K*_{tissue} and *p*_v were significantly higher, whereas φ and the OFC were significantly lower in treadmill noncompleters than in treadmill completers. Fifth, muscle perfusion parameters of the biomechanical model were significantly associated with the resting ABI, post-treadmill ABI, claudication onset time, and PWT in the pooled analysis comprising all study participants.

Conventional techniques to evaluate PAD are of limited ability to estimate diffuse or small vessel disease, or microvascular dysfunction, which are fundamental aspects of the pathophysiology of PAD.²³ Clinical studies have shown that perfusion imaging can evaluate PAD severity.²⁴ In a study of patients with PAD, perfusion deficits in the calf muscles and disease severity were determined by contrast-enhanced ultrasound.²⁵ A previous study

showed that patients with PAD with intermittent claudication compared with controls had lower peak exercise perfusion and lower limb perfusion.²³ Moreover, patients with PAD and diabetes were found to have poor tissue perfusion and flow impairment attributable to microvascular dysfunction. Perfusion imaging by contrast-enhanced ultrasound showed patients with diabetes with microvascular complications had reduced capillary volume recruitment.^{23,26} Muscle microvascular blood flow, oxygenation, and pH can act as surrogate markers for perfusion pressure. Previous studies showed that increased intramuscular pressure is associated with a significant decrease in muscle microvascular blood flow, oxygenation, pH, and perfusion pressure in the leg.²⁷ Hence, modeling parameters of microvascular perfusion could be useful to define disease severity including the influence of diabetes on lower extremity ischemia, as reported in this study. Meneses et al demonstrated a strong correlation

Table 6. Associations of Computational Microvascular Modeling Parameters From Controls With Markers of PAD

Variable	Independent variable	Obs	β	SE	R^2	Adjusted r^2	P value
k^t	Resting ABI	20	0.042	0.0591	0.03	-0.03	0.48
	Post-treadmill ABI	20	0.149	0.0557	0.29	0.25	0.015
	Δ of ABI	20	0.107	0.0783	0.09	0.04	0.19
	Claudication onset time, s	20	-9.855	12.786	0.03	-0.02	0.45
	Peak walking time, s	20	-9.855	12.786	0.03	-0.02	0.45
φ	Resting ABI	20	-0.967	0.5799	0.13	0.09	0.11
	Post-treadmill ABI	20	-1.097	0.6353	0.14	0.09	0.10
	Δ of ABI	20	-0.129	0.8550	0.00	-0.05	0.88
	Claudication onset time, s	20	-19.22	135.13	0.00	-0.05	0.89
	Peak walking time, s	20	-19.22	135.13	0.00	-0.05	0.89
OFC	Resting ABI	20	0.022	0.0067	0.37	0.33	0.005
	Post-treadmill ABI	20	0.017	0.0084	0.19	0.15	0.05
	Δ of ABI	20	-0.004	0.0116	0.01	-0.05	0.71
	Claudication onset time, s	20	0.777	1.8260	0.01	-0.05	0.68
	Peak walking time, s	20	0.777	1.8260	0.01	-0.05	0.68
p_v	Resting ABI	20	-0.014	0.0218	0.02	-0.03	0.51
	Post-treadmill ABI	20	-0.020	0.0238	0.04	-0.02	0.41
	Δ of ABI	20	-0.006	0.0302	0.00	-0.05	0.85
	Claudication onset time, s	20	-0.303	4.7780	0.00	-0.06	0.95
	Peak walking time, s	20	-0.303	4.7780	0.00	-0.06	0.95

Linear regression analyses were performed for controls. K_{tissue} is a constant for controls. ABI indicates ankle-brachial index; k^t , transfer rate constant; K_{tissue} , interstitial permeability; Obs, number of observations; OFC, outflow filtration coefficient; PAD, peripheral artery disease; p_v , microvascular pressure; Δ of ABI, difference between resting ankle-brachial index and post-treadmill ankle-brachial index; and φ , porosity.

between impaired muscle perfusion and disease severity in patients with PAD during postocclusion hyperemia.²⁸

Duscha et al showed an association of capillary density with claudication times and anaerobic threshold in patients with PAD.²⁹ Robbins et al³⁰ reported that leg muscle capillary density is associated with peak hyperemic blood flow in patients with lower extremity ischemia. These data indicate that microcirculatory changes contribute to functional impairment, which agrees with our findings.

Wu et al³¹ reported that differences in the composition of muscle fibers across various skeletal muscle

compartments and connective tissue could cause inhomogeneous muscle perfusion in healthy adults. We have also observed heterogeneous patterns of the modeling parameters across skeletal calf muscle compartments.

The estimation of capillary permeability allows for defining the inflammatory response and regenerative processes following muscle injury.³² Inflammation increased capillary permeability.³³ Shimotsu et al³⁴ showed that endothelial cell swelling corresponds to enhanced microvascular permeability which aligns with our finding that capillary permeability was higher in

Table 7. Computational Microvascular Model Parameters for Nondiabetic And Diabetic Patients With PAD

Variable	Nondiabetic group	Diabetic group	P value
k^t , 1/s	5.40 (3.97–6.83)	5.49 (4.37–6.60)	0.93
K_{tissue} , m ²	3.10 (2.62–3.57)	4.00 (3.44–4.56)	0.017
φ	0.55 (0.51–0.60)	0.51 (0.46–0.56)	0.21
OFC, 1/Pa s	11.82 (10.84–12.81)	12.07 (10.14–14.00)	0.79
p_v , mmHg	50.78 (49.92–51.64)	52.36 (51.09–53.64)	0.034

All values are expressed as median (interquartile range). P values were calculated with the Kruskal–Wallis rank test. Nondiabetic group: n=36; diabetic group: n=20. k^t indicates transfer rate constant; K_{tissue} , interstitial permeability; OFC, outflow filtration coefficient; PAD, peripheral artery disease; p_v , microvascular pressure; and φ , porosity (values in the range from 0 to 1).

Table 8. Computational Microvascular Model Parameters for PAD Treadmill Completers and Noncompleters

Variable	Completers	Noncompleters	P value
k^t , 1/s	6.15 (4.39–7.91)	8.13 (6.41–9.85)	0.10
K_{tissue} , m ²	3.72 (3.44–4.00)	4.98 (4.70–5.25)	<0.001
φ	0.53 (0.51–0.56)	0.40 (0.38–0.41)	<0.001
OFC, 1/Pa s	12.97 (12.00–13.94)	9.01 (7.14–10.88)	<0.001
p_v , mmHg	51.15 (49.78–52.52)	54.07 (53.60–54.55)	<0.001

All values are expressed as median (interquartile range). P values were calculated with the Kruskal–Wallis rank test. Completers PAD group: n=19; noncompleters PAD group: n=17. k^t indicates transfer rate constant; K_{tissue} , interstitial permeability; OFC, outflow filtration coefficient; PAD, peripheral artery disease; p_v , microvascular pressure; and φ , porosity (values in the range from 0 to 1).

patients with PAD than in matched controls. We further observed that capillary permeability and microvascular pressure were also higher in diabetes compared with patients with PAD without diabetes.

This study adds to the growing body of evidence on the importance of the microcirculation in PAD. Future work will need to further elucidate associations between the microcirculation and typical PAD symptoms, and to understand whether therapeutic interventions can sustainably alter microvascular blood flow in the lower extremities.

This study has limitations including a limited sample size. Patients with a contraindication to MRI or GBCAs were excluded from this study. Chronic kidney disease is significantly and independently associated with PAD, limiting the use of GBCA during MR imaging. The finite element model of muscle perfusion has limitations. Blood was assumed as a Newtonian fluid, and we did not include nonlinear reactions. However, we have previously reported that using a non-Newtonian model does not significantly affect the results.¹⁵ We have not tested interaction terms between clinical variables and the computational microvascular model parameters which will need to be investigated in larger future studies.

In conclusion, computational microvascular model parameters differed significantly between patients with PAD and matched controls. Thus, computational microvascular modeling could be of interest in studying lower extremity ischemia.

ARTICLE INFORMATION

Received July 27, 2022; accepted December 14, 2022.

Affiliations

Penn State Heart and Vascular Institute, Pennsylvania State University College of Medicine, Hershey, PA (O.A.G., G.B.); Section of Cardiovascular Research, Department of Medicine (C.M.S., A.A.T., V.N., J.D.M., C.M.B., G.B.), and Department of Medicine, Section of Cardiology (V.N., C.M.B.), Baylor College of Medicine, Houston, TX; Michael E DeBakey VA Medical Center, Houston, TX (A.A.T., V.N.); Methodist DeBakey Heart and Vascular Center, Houston Methodist Hospital, Houston, TX (T.B., D.J.S.); and Division of Vascular and Endovascular Surgery, Louisiana State University Health Sciences Center, New Orleans, LA (J.B.).

Acknowledgments

We thank all study participants for their cooperation.

Sources of Funding

This work was supported by funding from the National Institutes of Health (R01HL137763 and K25HL121149 both to GB) and the American Heart Association (13BGA16720014 to GB).

Disclosures

None.

Supplemental Material

Tables S1–S3

REFERENCES

- Brunner G, Bismuth J, Nambi V, Ballantyne CM, Taylor AA, Lumsden AB, Morrisett JD, Shah DJ. Calf muscle perfusion as measured with magnetic resonance imaging to assess peripheral arterial disease. *Med Biol Eng Comput*. 2016;54:1667–1681. doi: [10.1007/s11517-016-1457-1](https://doi.org/10.1007/s11517-016-1457-1)
- Kamran H, Nambi V, Negi S, Yang EY, Chen C, Virani SS, Kougias P, Lumsden AB, Morrisett JD, Ballantyne CM, et al. Magnetic resonance venous volume measurements in peripheral artery disease (from ELIMIT). *Am J Cardiol*. 2016;118:1399–1404. doi: [10.1016/j.amjcard.2016.07.051](https://doi.org/10.1016/j.amjcard.2016.07.051)
- Chen S, Tyan Y-C, Lai J-J, Chang C-C. Automated determination of arterial input function for dynamic susceptibility contrast MRI from regions around arteries using independent component analysis. *Radiol Res Pract*. 2016;2016:2657405. doi: [10.1155/2016/2657405](https://doi.org/10.1155/2016/2657405)
- Swartz RH, Bhuta SS, Farb RI, Agid R, Willinsky RA, Terbrugge KG, Butany J, Wasserman BA, Johnstone DM, Silver FL, et al. Intracranial arterial wall imaging using high-resolution 3-tesla contrast-enhanced MRI. *Neurology*. 2009;72:627–634. doi: [10.1212/01.wnl.0000342470.69739.b3](https://doi.org/10.1212/01.wnl.0000342470.69739.b3)
- Kleiss SF, Ma KF, El Moumni M, Unlu C, Nijboer TS, Schuurmann RCL, Bokkers RPH, de Vries JPM. Detecting changes in tissue perfusion with hyperspectral imaging and thermal imaging following endovascular treatment for peripheral arterial disease. *J Endovasc Ther*. 2022;15266028221082013. doi: [10.1177/15266028221082013](https://doi.org/10.1177/15266028221082013)
- Phelps EA, Garcia AJ. Update on therapeutic vascularization strategies. *Regen Med*. 2009;4:65–80. doi: [10.2217/17460751.4.1.65](https://doi.org/10.2217/17460751.4.1.65)
- Silva JA, White CJ, Quintana H, Collins TJ, Jenkins JS, Ramee SR. Percutaneous revascularization of the common femoral artery for limb ischemia. *Catheter Cardiovasc Interv*. 2004;62:230–233. doi: [10.1002/ccd.20035](https://doi.org/10.1002/ccd.20035)
- Stoner MC, Defreitas DJ, Manwaring MM, Carter JJ, Parker FM, Powell CS. Cost per day of patency: understanding the impact of patency and reintervention in a sustainable model of healthcare. *J Vasc Surg*. 2008;48:1489–1496. doi: [10.1016/j.jvs.2008.07.003](https://doi.org/10.1016/j.jvs.2008.07.003)
- Cibis M, Potters WV, Selwaness M, Gijzen FJ, Franco OH, Arias Lorza AM, de Bruijne M, Hofman A, van der Lugt A, Nederveen AJ, et al. Relation between wall shear stress and carotid artery wall thickening MRI versus CFD. *J Biomech*. 2016;49:735–741. doi: [10.1016/j.jbiomech.2016.02.004](https://doi.org/10.1016/j.jbiomech.2016.02.004)
- Hossain SS, Zhang Y, Fu X, Brunner G, Singh J, Hughes TJ, Shah D, Decuzzi P. Magnetic resonance imaging-based computational modeling of blood flow and nanomedicine deposition in patients with peripheral arterial disease. *J R Soc Interface*. 2015;12:20150001.
- Singh J, Brunner G, Morrisett JD, Ballantyne CM, Lumsden AB, Shah DJ, Decuzzi P. Patient-specific flow descriptors and normalized wall index in peripheral artery disease: a preliminary study. *Comput Methods Biomech Biomed Eng Imaging Vis*. 2018;6:119–127. doi: [10.1080/21681163.2016.1184589](https://doi.org/10.1080/21681163.2016.1184589)
- Debbaut C, Monbaliu D, Casteleyn C, Cornillie P, Van Loo D, Masschaele B, Pirenne J, Simoens P, Van Hoorebeke L, Segers P. From vascular corrosion cast to electrical analog model for the study of human liver hemodynamics and perfusion. *IEEE Trans Biomed Eng*. 2011;58:25–35. doi: [10.1109/TBME.2010.2065229](https://doi.org/10.1109/TBME.2010.2065229)
- Rani HP, Sheu TW, Chang TM, Liang PC. Numerical investigation of non-Newtonian microcirculatory blood flow in hepatic lobule. *J Biomech*. 2006;39:551–563. doi: [10.1016/j.jbiomech.2004.11.029](https://doi.org/10.1016/j.jbiomech.2004.11.029)
- van der Plaats A, t Hart NA, Verkerke GJ, Leuvenink HG, Verdonck P, Ploeg RJ, Rakhorst G. Numerical simulation of the hepatic circulation. *Int J Artif Organs*. 2004;27:222–230. doi: [10.1177/039139880402700309](https://doi.org/10.1177/039139880402700309)
- Gimnich OA, Singh J, Bismuth J, Shah DJ, Brunner G. Magnetic resonance imaging based modeling of microvascular perfusion in patients with peripheral artery disease. *J Biomech*. 2019;93:147–158. doi: [10.1016/j.jbiomech.2019.06.025](https://doi.org/10.1016/j.jbiomech.2019.06.025)
- Gimnich OA, Holbrook J, Belousova T, Short CM, Taylor AA, Nambi V, Morrisett JD, Ballantyne CM, Bismuth J, Shah DJ, et al. Relation of magnetic resonance imaging based arterial signal enhancement to markers of peripheral artery disease. *Am J Cardiol*. 2021;140:140–147. doi: [10.1016/j.amjcard.2020.10.049](https://doi.org/10.1016/j.amjcard.2020.10.049)
- Tofts PS, Kermode AG. Measurement of the blood-brain barrier permeability and leakage space using dynamic MR imaging. 1. Fundamental concepts. *Magn Reson Med*. 1991;17:357–367. doi: [10.1002/mrm.1910170208](https://doi.org/10.1002/mrm.1910170208)
- Pishko GL, Astary GW, Zhang J, Mareci TH, Sarntinoranont M. Role of convection and diffusion on DCE-MRI parameters in low leakiness

- KHT sarcomas. *Microvasc Res*. 2012;84:306–313. doi: [10.1016/j.mvr.2012.09.001](https://doi.org/10.1016/j.mvr.2012.09.001)
19. Tofts PS, Brix G, Buckley DL, Evelhoch JL, Henderson E, Knopp MV, Larsson HB, Lee TY, Mayr NA, Parker GJ, et al. Estimating kinetic parameters from dynamic contrast-enhanced T(1)-weighted MRI of a diffusable tracer: standardized quantities and symbols. *J Magn Reson Imaging*. 1999;10:223–232. doi: [10.1002/\(SICI\)1522-2566\(199909\)10:3<223::AID-JMRI>3.0.CO;2-S](https://doi.org/10.1002/(SICI)1522-2566(199909)10:3<223::AID-JMRI>3.0.CO;2-S)
 20. Pishko GL, Astarly GW, Mareci TH, Sarntinoranont M. Sensitivity analysis of an image-based solid tumor computational model with heterogeneous vasculature and porosity. *Ann Biomed Eng*. 2011;39:2360–2373. doi: [10.1007/s10439-011-0349-7](https://doi.org/10.1007/s10439-011-0349-7)
 21. Smye SW, Evans CJ, Robinson MP, Sleeman BD. Modelling the electrical properties of tissue as a porous medium. *Phys Med Biol*. 2007;52:7007–7022. doi: [10.1088/0031-9155/52/23/016](https://doi.org/10.1088/0031-9155/52/23/016)
 22. Thompson RB, Aviles RJ, Faranesh AZ, Raman VK, Wright V, Balaban RS, McVeigh ER, Lederman RJ. Measurement of skeletal muscle perfusion during postischemic reactive hyperemia using contrast-enhanced MRI with a step-input function. *Magn Reson Med*. 2005;54:289–298. doi: [10.1002/mrm.20535](https://doi.org/10.1002/mrm.20535)
 23. Nguyen T, Davidson BP. Contrast enhanced ultrasound perfusion imaging in skeletal muscle. *J Cardiovasc Imaging*. 2019;27:163–177. doi: [10.4250/jcvi.2019.27.e31](https://doi.org/10.4250/jcvi.2019.27.e31)
 24. Amarteifio E, Wormsbecher S, Krix M, Demirel S, Braun S, Delorme S, Bockler D, Kauczor HU, Weber MA. Dynamic contrast-enhanced ultrasound and transient arterial occlusion for quantification of arterial perfusion reserve in peripheral arterial disease. *Eur J Radiol*. 2012;81:3332–3338. doi: [10.1016/j.ejrad.2011.12.030](https://doi.org/10.1016/j.ejrad.2011.12.030)
 25. Duerschmied D, Maletzki P, Freund G, Olschewski M, Bode C, Hehrlein C. Success of arterial revascularization determined by contrast ultrasound muscle perfusion imaging. *J Vasc Surg*. 2010;52:1531–1536. doi: [10.1016/j.jvs.2010.07.010](https://doi.org/10.1016/j.jvs.2010.07.010)
 26. Eggleston EM, Jahn LA, Barrett EJ. Hyperinsulinemia rapidly increases human muscle microvascular perfusion but fails to increase muscle insulin clearance: evidence that a saturable process mediates muscle insulin uptake. *Diabetes*. 2007;56:2958–2963. doi: [10.2337/db07-0670](https://doi.org/10.2337/db07-0670)
 27. Challa ST, Hargens AR, Uzosike A, Macias BR. Muscle microvascular blood flow, oxygenation, pH, and perfusion pressure decrease in simulated acute compartment syndrome. *J Bone Joint Surg Am*. 2017;99:1453–1459. doi: [10.2106/JBJS.16.01191](https://doi.org/10.2106/JBJS.16.01191)
 28. Meneses AL, Nam MCY, Bailey TG, Magee R, Golledge J, Hellsten Y, Keske MA, Greaves K, Askew CD. Leg blood flow and skeletal muscle microvascular perfusion responses to submaximal exercise in peripheral arterial disease. *Am J Physiol Heart Circ Physiol*. 2018;315:H1425–H1433. doi: [10.1152/ajpheart.00232.2018](https://doi.org/10.1152/ajpheart.00232.2018)
 29. Duscha BD, Kraus WE, Jones WS, Robbins JL, Piner LW, Huffman KM, Allen JD, Annex BH. Skeletal muscle capillary density is related to anaerobic threshold and claudication in peripheral artery disease. *Vasc Med*. 2020;25:411–418. doi: [10.1177/1358863X20945794](https://doi.org/10.1177/1358863X20945794)
 30. Robbins JL, Jones WS, Duscha BD, Allen JD, Kraus WE, Regensteiner JG, Hiatt WR, Annex BH. Relationship between leg muscle capillary density and peak hyperemic blood flow with endurance capacity in peripheral artery disease. *J Appl Physiol*. 2011;111:81–86. doi: [10.1152/jappphysiol.00141.2011](https://doi.org/10.1152/jappphysiol.00141.2011)
 31. Wu WC, Wang J, Detre JA, Wehrli FW, Mohler E 3rd, Ratcliffe SJ, Floyd TF. Hyperemic flow heterogeneity within the calf, foot, and forearm measured with continuous arterial spin labeling MRI. *Am J Physiol Heart Circ Physiol*. 2008;294:H2129–H2136. doi: [10.1152/ajpheart.01399.2007](https://doi.org/10.1152/ajpheart.01399.2007)
 32. Hotta K, Behnke BJ, Masamoto K, Shimotsu R, Onodera N, Yamaguchi A, Poole DC, Kano Y. Microvascular permeability of skeletal muscle after eccentric contraction-induced muscle injury: in vivo imaging using two-photon laser scanning microscopy. *J Appl Physiol (Bethesda, MD: 1985)*. 2018;125:369–380. doi: [10.1152/jappphysiol.00046.2018](https://doi.org/10.1152/jappphysiol.00046.2018)
 33. Soeters PB, Wolfe RR, Shenkin A. Hypoalbuminemia: pathogenesis and clinical significance. *J Parenter Enteral Nutr*. 2019;43:181–193. doi: [10.1002/jpen.1451](https://doi.org/10.1002/jpen.1451)
 34. Shimotsu R, Hotta K, Ikegami R, Asamura T, Tabuchi A, Masamoto K, Yagishita K, Poole DC, Kano Y. Vascular permeability of skeletal muscle microvessels in rat arterial ligation model: in vivo analysis using two-photon laser scanning microscopy. *Am J Physiol Regul Integr Comp Physiol*. 2021;320:R972–R983. doi: [10.1152/ajpregu.00135.2020](https://doi.org/10.1152/ajpregu.00135.2020)

Supplemental Material

Table S1. Computational microvascular model parameters of PAD patients and controls for skeletal calf muscle compartments.

Variable	Muscle group	Control	PAD	Pooled	P-Value
k^t (1/s)	AM	2.80 (2.36, 3.24)	11.50 (7.52, 15.49)	8.39 (5.63, 11.16)	0.018
	LM	2.45 (2.08, 2.81)	7.46 (3.83, 11.09)	5.67 (3.28, 8.05)	0.042
	DM	3.26 (2.95, 3.57)	6.76 (6.10, 7.42)	5.51 (4.89, 6.13)	<0.001
	SM	2.42 (2.15, 2.69)	6.00 (5.33, 6.67)	4.72 (4.09, 5.35)	<0.001
	GM	1.34 (1.09, 1.58)	3.71 (2.15, 5.26)	2.86 (1.83, 3.89)	0.026
K_{tissue} (m^2)	AM	1.81 (1.81, 1.81)	5.46 (4.95, 5.96)	4.15 (3.58, 4.72)	<0.001
	LM	1.81 (1.81, 1.81)	3.63 (3.35, 3.92)	2.98 (2.69, 3.28)	<0.001
	DM	1.81 (1.81, 1.81)	4.07 (3.65, 4.50)	3.27 (2.87, 3.66)	<0.001
	SM	1.81 (1.81, 1.81)	3.69 (3.40, 3.98)	3.02 (2.72, 3.33)	<0.001
	GM	1.81 (1.81, 1.81)	4.71 (4.00, 5.42)	3.68 (3.09, 4.26)	<0.001
ϕ	AM	0.61 (0.61, 0.62)	0.43 (0.39, 0.46)	0.49 (0.46, 0.53)	<0.001
	LM	0.61 (0.59, 0.62)	0.56 (0.54, 0.57)	0.57 (0.56, 0.59)	<0.001
	DM	0.67 (0.65, 0.70)	0.48 (0.44, 0.53)	0.55 (0.51, 0.59)	<0.001
	SM	0.63 (0.62, 0.64)	0.44 (0.41, 0.48)	0.51 (0.48, 0.54)	<0.001
	GM	0.83 (0.77, 0.88)	0.43 (0.39, 0.47)	0.57 (0.51, 0.63)	<0.001
OFC (1/Pa s)	AM	12.62 (10.22, 15.02)	8.05 (6.72, 9.39)	9.68 (8.38, 10.99)	0.001
	LM	13.60 (11.74, 15.46)	12.96 (10.93, 15.00)	13.19 (11.76, 14.63)	0.67
	DM	13.85 (12.19, 15.51)	11.31 (9.42, 13.19)	12.21 (10.86, 13.57)	0.07
	SM	13.88 (12.38, 15.38)	11.88 (9.96, 13.79)	12.59 (11.26, 13.93)	0.15
	GM	12.92 (11.36, 14.48)	11.29 (10.04, 12.55)	11.87 (10.90, 12.85)	0.11
p_v (mmHg)	AM	49.33 (48.81, 49.85)	51.22 (49.75, 52.69)	50.54 (49.57, 51.52)	0.06
	LM	49.00 (48.07, 49.93)	52.51 (50.72, 54.30)	51.26 (50.00, 52.51)	0.006
	DM	49.16 (48.82, 49.50)	57.79 (55.01, 58.56)	54.06 (52.57, 55.56)	<0.001
	SM	49.23 (48.55, 49.92)	50.64 (49.60, 51.69)	50.14 (49.42, 50.86)	0.06
	GM	49.32 (48.63, 50.01)	51.50 (50.43, 52.56)	50.72 (49.95, 51.49)	0.005

All values are expressed as medians and interquartile ranges (IQRs). P-values were calculated with the Kruskal-Wallis rank test. Control group: $n = 20$; PAD group: $n = 36$. Leg muscle groups: AM: anterior muscle, LM: lateral muscle, DM: deep posterior muscle, SM: soleus muscle, GM: gastrocnemius muscle. k^t , transfer rate constant; K_{tissue} , interstitial permeability; ϕ , porosity (values in the range from 0 to 1); OFC, outflow filtration coefficient; p_v , microvascular pressure. PAD: peripheral artery disease. Pooled: includes both PAD patients and controls.

Table S2. Computational microvascular model parameters of non-diabetic and diabetic study participants for skeletal calf muscle compartments.

Variable	Muscle group	Non-diabetics	Diabetics	P-value
k^i (1/s)	AM	8.57 (4.38, 12.77)	8.07 (5.74, 10.40)	0.86
	LM	5.85 (2.34, 9.36)	5.34 (2.71, 7.97)	0.84
	DM	5.12 (4.36, 5.88)	6.21 (5.10, 7.31)	0.10
	SM	4.46 (3.66, 5.26)	5.20 (4.09, 6.30)	0.27
	GM	3.00 (1.38, 4.61)	2.62 (2.14, 3.10)	0.73
K_{tissue} (m^2)	AM	3.58 (2.92, 4.23)	5.19 (4.21, 6.17)	0.005
	LM	2.70 (2.35, 3.05)	3.50 (3.00, 4.00)	0.009
	DM	2.89 (2.46, 3.31)	3.95 (3.17, 4.73)	0.009
	SM	2.77 (2.40, 3.13)	3.48 (2.97, 4.00)	0.023
	GM	3.55 (2.81, 4.29)	3.90 (2.86, 4.93)	0.58
φ	AM	0.50 (0.46, 0.54)	0.48 (0.41, 0.54)	0.44
	LM	0.58 (0.56, 0.59)	0.57 (0.55, 0.60)	0.70
	DM	0.55 (0.51, 0.60)	0.54 (0.47, 0.61)	0.80
	SM	0.52 (0.48, 0.56)	0.49 (0.44, 0.55)	0.39
	GM	0.62 (0.54, 0.69)	0.48 (0.38, 0.58)	0.026
OFC (1/Pa s)	AM	9.96 (8.20, 11.72)	9.19 (7.16, 11.22)	0.58
	LM	12.64 (11.22, 14.06)	14.18 (10.91, 17.46)	0.31
	DM	11.87 (10.66, 13.08)	12.83 (9.52, 16.14)	0.50
	SM	12.58 (11.08, 14.08)	12.62 (9.81, 15.42)	0.98
	GM	12.06 (10.91, 13.22)	11.53 (9.62, 13.45)	0.61
p_v (mmHg)	AM	50.00 (49.07, 50.93)	51.52 (49.28, 53.76)	0.14
	LM	51.15 (49.77, 52.52)	51.46 (48.75, 54.17)	0.82
	DM	52.55 (51.00, 54.09)	56.80 (53.85, 59.75)	0.005
	SM	49.65 (48.75, 50.56)	51.01 (49.79, 52.23)	0.07
	GM	50.55 (49.77, 51.32)	51.03 (49.28, 52.77)	0.56

All values are medians and interquartile range (IQR). P-values were calculated with the Kruskal-Wallis rank test. Non-diabetics group: $n = 36$; diabetics group: $n = 20$. Leg muscle groups: AM: anterior muscle, LM: lateral muscle, DM: deep posterior muscle, SM: soleus muscle, GM: gastrocnemius muscle. k^i , transfer rate constant; K_{tissue} , interstitial permeability; φ , porosity (values in the range from 0 to 1); OFC, outflow filtration coefficient; p_v , microvascular pressure; PAD: peripheral artery disease.

Table S3. Computational microvascular model parameters of PAD treadmill completers and non-completers for skeletal calf muscle compartments.

Variable	Muscle group	Completers	Non-Completers	P-value
k^t (1/s)	AM	10.03 (2.63, 17.43)	13.15 (10.18, 16.11)	0.44
	LM	6.57 (2.71, 10.42)	8.45 (1.60, 15.31)	0.61
	DM	5.54 (4.65, 6.44)	8.12 (7.70, 8.53)	<0.001
	SM	4.71 (3.98, 5.44)	7.44 (6.76, 8.12)	<0.001
	GM	3.89 (0.81, 6.98)	3.50 (3.38, 3.63)	0.80
K_{tissue} (m ²)	AM	4.82 (4.18, 5.47)	6.16 (5.47, 6.86)	0.005
	LM	3.27 (2.79, 3.75)	4.04 (3.88, 4.20)	0.004
	DM	3.75 (2.99, 4.50)	4.44 (4.09, 4.79)	0.10
	SM	3.35 (2.98, 3.73)	4.08 (3.67, 4.48)	0.009
	GM	3.41 (2.58, 4.23)	6.17 (5.45, 6.89)	<0.001
ϕ	AM	0.49 (0.44, 0.53)	0.36 (0.33, 0.40)	<0.001
	LM	0.58 (0.56, 0.60)	0.53 (0.51, 0.55)	<0.001
	DM	0.57 (0.53, 0.62)	0.38 (0.34, 0.42)	<0.001
	SM	0.50 (0.46, 0.55)	0.38 (0.35, 0.40)	<0.001
	GM	0.51 (0.46, 0.56)	0.34 (0.31, 0.36)	<0.001
OFC (1/Pa s)	AM	7.16 (4.95, 9.38)	9.05 (7.56, 10.54)	0.16
	LM	15.40 (13.56, 17.24)	10.25 (6.68, 13.81)	0.008
	DM	13.15 (11.03, 15.27)	9.24 (6.09, 12.39)	0.033
	SM	15.42 (13.97, 16.88)	7.92 (5.18, 10.65)	<0.001
	GM	13.71 (12.26, 15.16)	8.59 (7.41, 9.77)	<0.001
p_v (mmHg)	AM	49.90 (47.52, 52.27)	52.69 (51.10, 54.29)	0.05
	LM	51.48 (48.76, 54.20)	53.66 (51.22, 56.11)	0.22
	DM	54.62 (51.92, 57.32)	59.21 (57.35, 61.07)	0.007
	SM	49.74 (47.94, 51.54)	51.65 (50.73, 52.57)	0.06
	GM	50.01 (48.37, 51.66)	53.16 (52.26, 54.06)	0.002

All values are medians and interquartile range (IQR). P-values were calculated with the Kruskal-Wallis rank test. Completers PAD group: $n = 19$; Non-completers PAD group: $n = 17$. Leg muscle groups: AM: anterior muscle, LM: lateral muscle, DM: deep posterior muscle, SM: soleus muscle, GM: gastrocnemius muscle. k^t , transfer rate constant; K_{tissue} , interstitial permeability; ϕ , porosity (values in the range from 0 to 1); OFC, outflow filtration coefficient; p_v , microvascular pressure; PAD: peripheral artery disease.